

GMT: Guided Mask Transformer for Leaf Instance Segmentation

Feng Chen¹

Feng.Chen@ed.ac.uk

Sotirios A. Tsafaris¹

S.Tsafaris@ed.ac.uk

Mario Valerio Giuffrida²

Valerio.Giuffrida@nottingham.ac.uk

¹ School of Engineering
University of Edinburgh
United Kingdom

² School of Computer Science
University of Nottingham
United Kingdom

Abstract

Leaf instance segmentation is a challenging multi-instance segmentation task, aiming to separate and delineate each leaf in an image of a plant. The delineation of each leaf is a necessary prerequisite task for several biology-related applications such as the fine-grained monitoring of plant growth, and crop yield estimation. The task is challenging because self-similarity of instances is high (similar shape and colour) and instances vary greatly in size under heavy occlusion.

We believe that the key to overcoming the aforementioned challenges lies in the specific spatial patterns of leaf distribution. For example, leaves typically grow around the plant's center, with smaller leaves clustering and overlapped near this central point. In this paper, we propose a novel approach named Guided Mask Transformer (GMT), which contains three key components, namely Guided Positional Encoding (GPE), Guided Embedding Fusion Module (GEFM) and Guided Dynamic Positional Queries (GDPQ), to extend the meta-architecture of Mask2Former and incorporate with a set of harmonic guide functions. These guide functions are tailored to the pixel positions of instances and trained to separate distinct instances in an embedding space. The proposed GMT consistently outperforms State-of-the-Art models on three public plant datasets.

1 Introduction

Plant phenotyping is the process to measure physical traits of plants, such as height, leaf area and flowering time. In recent years, computer vision and machine learning have advanced plant analysis for phenotyping and accelerated scientific discoveries for the plant community [24]. In this paper, we focus on the image-based analysis of plant leaves as a non-destructive approach to plant phenotyping. The quantification of plant leaves is important to reveal several characteristics, such as respiration, nutrition, and photosynthesis [2].

Instance segmentation is a computer vision task that has been extensively studied [15, 30]. With the rise of Transformers [12, 36], State-of-the-Art (SotA) Transformer-based models have surpassed the performance of convolutional neural networks in many tasks. Yet, these models still face challenges in achieving robust instance segmentation on plant leaves, despite the overall advancements. In fact, plants pose a challenge to computer vision models due to their complexity, as plants exhibit severe overlaps and a huge intra- and inter-species morphological variability [63]. The challenges arising from leaf instance segmentation have

arXiv:2406.17109v1 [cs.CV] 24 Jun 2024

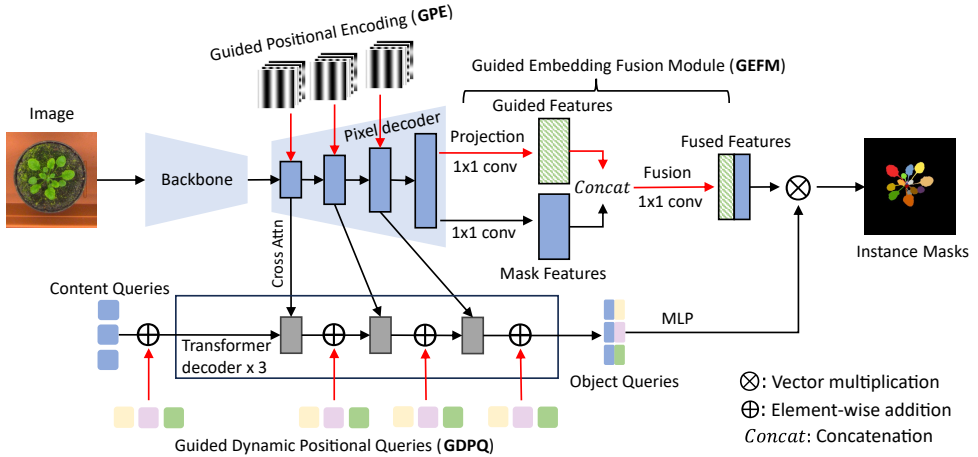


Figure 1: A pictorial representation of our method, the Guided Mask Transformer (GMT). The key components of GMT are the Guided Positional Encoding (GPE), the Guided Embedding Fusion Module (GEFM), and the Guided Dynamic Positional Queries (GDPQ). These components enable an effective integration with the guide functions carrying prior knowledge on instances’ distribution. (Best viewed in colour.)

been extensively studied for years in the CVPPP/CVPPA series of workshops.¹

In this paper, we present the Guided Mask Transformer (GMT), a Transformer-based model specifically tailored to instance segmentation on plant images (Figure 1). Our model extends Mask2Former [9] with three key designs, namely Guided Positional Encoding (GPE), Guided Embedding Fusion Module (GEFM) and Guided Dynamic Positional Queries (GDPQ), in which we integrate prior knowledge on the spatial distributions of leaf instances. In particular, we leverage a set of guide functions to learn this prior knowledge before the integration. Experimental results on three well-known plant datasets show that GMT outperforms the SotA models. Furthermore, we demonstrate the potential of our approach through an ablation study, showing the impact of each key component to the learning process.

In summary, the major contributions of this work are: (i) We propose GMT, as a novel way of utilising the priori of instances’ distribution to facilitate the learning of leaf instance segmentation in a Transformer-based model; (ii) We demonstrate SotA performance of the proposed GMT on three public datasets, with ablative experiments showing the necessity of key design.

2 Related Work

We first review plant image segmentation approaches and, since our approach is based on Transformers, we review recent works in Transformer-based segmentation methods.

Plant Image Segmentation. Plant image segmentation plays a key role in various agricultural and plant phenotyping applications. Advanced computer vision and machine learning techniques have been extensively used in this domain. For instance, Singh & Misra [24]

¹<https://cvppa2021.github.io/challenges/>

leverage image segmentation methods to detect leaf diseases. Zhang *et al.* [42] propose a wheat spikelet instance segmentation method based on the hybrid task cascade model [6]. Jia *et al.* [24] propose the FoveaMask for fast instance segmentation on green fruits. With the recent advance of Transformers, an increasing number of works also leverage Transformer-based models in plant image segmentation [8, 24, 22]. In this paper, we focus on leaf instance segmentation using a Transformer-based model.

Transformer-based Segmentation. The Transformer has been successfully applied across various domains of machine learning, including NLP [8, 22] and computer vision [6, 23, 52]. As the Detection Transformer (DETR) [4] demonstrated superior performance and ease of use in object detection, many following studies have adopted similar principles to tackle image segmentation. MaskFormer [8] leverages a Transformer decoder to refine a set of object queries via cross attention and self attention, and these refined object queries are used to produce semantic masks. Mask2Former [9] proposes the masked cross attention to reduce computational burden and increase segmentation quality. In addition, it extends MaskFormer’s ability to perform semantic, instance, and panoptic segmentation individually. Furthermore, He *et al.* [16] introduce focus-aware dynamic positional queries alongside a method for performing cross-attention with high-resolution feature maps, both of which are crucial for image segmentation. FastInst [27] proposes a simple framework to perform real-time instance segmentation. OneFormer [20] is another powerful Transformer-based model that is trained only once, yet capable of performing all different segmentation tasks simultaneously. In this paper, we extend Mask2Former and propose the Guided Mask Transformer (GMT), which incorporates guide functions with spatial priors for leaf instance segmentation.

3 Proposed Method

Main idea. We aim to devise a method that effectively represents leaf and plant characteristics and integrates these characteristics into a representation that can be used by a segmentation model. To achieve this, our approach includes two crucial steps. Firstly, we employ a set of guide functions, which are adjusted to the pixel coordinates of different instances; these guide functions are optimised to separate distinct instances within an embedding space. Subsequently, the proposed Guided Mask Transformer (GMT), depicted in Figure 1, leverages the optimised guide functions, which possess priori of instance distribution, to train predicting instance masks of plant leaves.

3.1 Guide Functions

We start with a brief background on guide functions. The essence of the guide functions lies in their relevance to instance locations and the ability to separate distinct instances in an embedding space (after training). To this end, we adopt the harmonic functions [23] as guide functions, which are adjusted to pixel positions. The harmonic functions are defined as:

$$f_i(x, y; \psi_i) = \sin \left(\frac{\psi_i[1]}{W}x + \frac{\psi_i[2]}{H}y + \psi_i[3] \right), \quad (1)$$

where $\psi_i[1]$ and $\psi_i[2]$ are the learnable frequency parameters, $\psi_i[3]$ is the learnable phase parameter; W and H represent the image size; x and y denote the pixel coordinate. Given a

set of pixels S belong to an object, we can calculate the expectation of f_i over this object:

$$e_i(S; \psi_i) = \frac{1}{|S|} \sum_{(x,y) \in S} f_i(x, y; \psi_i). \quad (2)$$

Assuming the number of guide functions is d_g , the embedding of an object (we refer it as the guided embedding following [23]) is represented as a joint vector:

$$e(S; \Psi) = \{e_1(S; \psi_1), e_2(S; \psi_2), \dots, e_{d_g}(S; \psi_{d_g})\}. \quad (3)$$

The guide functions are trained to separate the guided embedding of different instances to a pre-set distance ε , and the loss function is defined as:

$$\ell(\Psi) = \sum_{I \in \mathcal{I}} \frac{1}{|P_I|} \sum_{(S, S') \in P_I} \max(0, \varepsilon - \|e(S; \Psi) - e(S'; \Psi)\|_1), \quad (4)$$

where \mathcal{I} denotes the set of training images, P_I represents all pairs of objects within an image I , S and S' are pixels belong to two different objects, and $\|\cdot\|_1$ is the L_1 distance.

3.2 GMT: Guided Mask Transformer

After learning the guide functions, we incorporate them into the proposed GMT model. One of our main contributions are the mechanisms we introduce to fully leverage the presence of these functions within a Mask2Former architecture [9].

Mask2Former preliminaries. Mask2Former consists of a backbone to extract image features, a pixel decoder to generate multi-scale pixel features, and a Transformer decoder to refine object queries through cross-attention with the multi-scale pixel features and self-attention blocks. Finally, instance masks are predicted by multiplying the object queries with the mask features (which are projected from the highest-resolution pixel features).

Guided Mask Transformer. Our GMT follows the standard design of Mask2Former, using the multi-scale deformable attention Transformer (MSDeformAttn) [43] as the pixel decoder, and the Transformer decoder is comprised of nine blocks, each containing a masked cross attention layer, a self attention layer, and a feed-forward layer. Deep supervision is employed after each block of the Transformer decoder. Below we describe the key components of GMT, which replace or enhance parts of the pixel decoder and Transformer decoder of Mask2Former. These adaptations enable the effective integration of the guide functions obtained from the previous stage. The architecture of GMT is shown in Figure 1.

Guided Positional Encoding (GPE). By default, sinusoidal positional encoding (SPE) [66] is added to the multi-scale pixel features at the pixel decoder in Mask2Former, defined as:

$$\text{SPE}_{pos, 2j} = \sin\left(\frac{pos}{10000^{2j/d_p}}\right), \quad \text{SPE}_{pos, 2j+1} = \cos\left(\frac{pos}{10000^{2j/d_p}}\right), \quad (5)$$

where d_p denotes the dimension of pixel features, $j \in [0, d_p/2 - 1]$ represents the index of the dimension of SPE and pos denotes pixel coordinates (*i.e.* x or y). Typically, $pos = x$ when $j < d_p/4$, otherwise $pos = y$.

As shown in Equation (1), the guide functions are sinusoidal and tailored to correspond with the pixel coordinates of instances. We hypothesise that the trained guide functions possess prior knowledge of the spatial distribution of different instances, which can improve

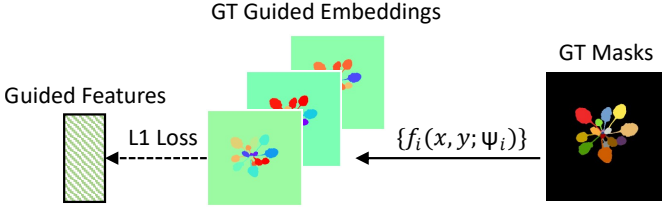


Figure 2: Auxiliary supervision at GEFM. The ground-truth (GT) instance masks are encoded by the trained guide functions to produce the GT guided embeddings. The guided features, which are projected from the final output of pixel decoder, are intermediately supervised by these embeddings.

the representation of the original SPE. However, the number of guide functions d_g is much less than d_p ; for instance, in our experiments, $d_g = 16$ and $d_p = 256$. To address this, we expand the number of guide functions to d_p by maintaining the frequency components $\psi[1]$ and $\psi[2]$, while shifting the phase components $\psi[3]$. Specifically, every guide function f_i is extended to $K = d_p/d_g$ functions, defined as:

$$f_{i,k}(x, y; \psi_i, k) = \sin\left(\frac{\psi_i[1]}{W}x + \frac{\psi_i[2]}{H}y + \psi_i[3] + 2\pi\frac{d_g k}{d_p}\right), \quad (6)$$

where $k = 0, 1, 2, \dots, K - 1$. The expanded set of guide functions is denoted as:

$$\mathcal{F} = \{f_{0,0}, f_{0,1}, \dots, f_{0,K-1}, f_{1,0}, f_{1,1}, \dots, f_{1,K-1}, \dots, f_{d_g-1,0}, f_{d_g-1,1}, \dots, f_{d_g-1,K-1}\}. \quad (7)$$

The concatenation of all elements in \mathcal{F} is then added to SPE to form the Guided Positional Encoding (GPE).

Guided Embedding Fusion Module (GEFM). As shown in Eq. 4, the trained guide functions are able to map the instance masks to guided embeddings where different objects are well separated. To facilitate this mapping in GMT, we simply add a 1×1 convolution layer to project the outputs of the pixel decoder to these embeddings, supervised by the ground-truth guided embeddings (which is generated by encoding the ground-truth instance masks with the trained guide functions) and an L_1 loss², as shown in Figure 2. Another 1×1 convolution layer is employed to merge the projected features with the original mask features.

Guided Dynamic Positional Queries (GDPQ). The Transformer decoder of Mask2Former progressively refines a set of randomly initialised object queries via attention mechanisms. These queries are formed as the addition of content queries, which are closely related objects' semantics, and positional queries, which are more relevant to instances' locations. Inspired by [16], we propose a novel way to dynamically generate the positional queries, conditioned on the guide functions, termed Guided Dynamic Positional Queries (GDPQ). The key contribution of [16] is the method to modulate positional queries using cross-attention maps; in particular, the positional queries Q_p at current block t are updated as:

$$Q_p^t = h(A^{t-1}K_p^{t-1} + B), \quad (8)$$

where h is an MLP, A^{t-1} and K_p^{t-1} denotes the cross-attention maps and positional encodings of pixel features (*i.e.* SPE) from the last block, respectively, and B is a bias term.

²Following the implementation in [16], we apply higher weights on the pixels of object edges.

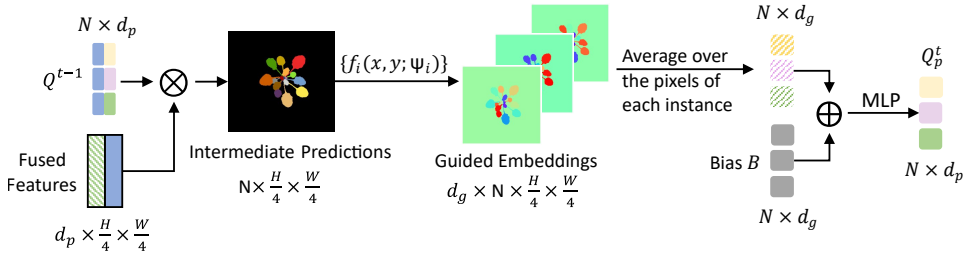


Figure 3: GDPQ Module. The positional queries at current Transformer block Q_p^t is dynamically generated on the guide-function-encoded mask predictions from the last block. Q^{t-1} denotes the object queries from the last Transformer block. The dimensions of different elements are shown. N is the length of object queries, and H and W denote the image size.

In our case, as the trained guide functions possess location prior of instances, we directly encode the intermediate predictions of GMT using the guide functions, and use it to generate the positional queries, as shown in Figure 3. The proposed GDPQ is expressed as:

$$Q_p^t = h(\mathcal{E}(S^{t-1}; \Psi) + B), \quad (9)$$

where S^{t-1} denotes the set of predicted instance masks from the previous Transformer block, and $\mathcal{E}(S^{t-1}; \Psi) = \text{Concat}_{S \in S^{t-1}} e(S; \Psi)$ represents the concatenation of all guided embeddings of these masks, as defined in Eq. 3. We configure $h(\cdot)$ as a three-layer MLP to map the concatenated embeddings to the same dimension of the object queries (*i.e.* mapping from 16 to 256). In this manner, the positional queries are conditioned on the guide functions, which embody positional priors, and are dynamically generated based on intermediate mask predictions, which continue to refine as the Transformer decoder progresses deeper. Finally, GDPQ and the content queries are summed up and processed by Transformer blocks.

4 Experimental Results

In this section, we discuss the experimental details and results on three public datasets, where the proposed GMT is compared with the baseline (*i.e.* Mask2Former) and other recent methods addressing the leaf instance segmentation task. Ablation studies are also conducted to demonstrate the efficacy of different components introduced in GMT.

4.1 Datasets

CVPPP LSC A1. The CVPPP 2017 Leaf Segmentation Challenge dataset (CVPPP LSC) [10] is a widely used dataset to benchmark leaf instance segmentation algorithms. We conduct experiments on the most commonly used subset, A1, which consists of a training set of 128 images and a hidden test set of 33 images. The size of each image is 500×530 pixels. We form a validation set by randomly selecting 12 images from the training set. Experimental results are reported on the hidden test set.

MSU-PID Arabidopsis. The Michigan State University Plant Imagery Database (MSU-PID) [11] consists of a subset of Arabidopsis plants and another subset of beans. We use the Arabidopsis subset containing 576 annotated images of 116×119 pixel resolution, which

are evenly distributed in 16 different plants. We randomly select 11, 2, and 3 different plants to form the training set, validation set, and test set, respectively. Repeated experiments are performed over 3 different data splits, and the average results on the test sets are reported.

KOMATSUNA RGB. The KOMATSUNA dataset [65] is formed by two subsets: one consists of RGB images and the other contains RGB-D images. Our experiments are performed on the RGB subset, which consists of 900 480×480 -pixel images evenly captured from 5 different plants. We divide the dataset into the training set, validation set and test set by randomly selecting 3, 1, and 1 different plants, respectively. Repeated experiments are performed over 3 different data splits, and the average results on the test sets are reported.

4.2 Implementation Details

Model Settings. By default, both the baseline model (Mask2Former) and the proposed GMT use the ResNet-50 [18] backbone. We evaluate other backbone options (ResNet-101 and Swin Transformer [27]) on GMT at the ablation study. As the number of training images of a leaf dataset is typically small (e.g. only a few hundred), the baseline model and GMT³ are pre-trained on COCO instance segmentation dataset [25].

Data Augmentation. We apply same data augmentation techniques to all the three datasets: random horizontal and vertical flips, followed by random scaled cropping. The input image sizes for CVPPP LSC A1, KOMATSUNA RGB, and MSU-PID are set to 512×512 , 480×480 , and 256×256 , respectively.

Training Strategies. When training the guide functions, we set the number of guide functions $d_g = 16$ and the distance to separate different instances $\varepsilon = 2$. Let $i \in [0, d_g - 1]$ be the index of a guide function, the learnable parameters ψ are randomly initialised as:

$$\begin{cases} \psi_i[1] \sim U(0, 50), \quad \psi_i[2] = 0, \quad \psi_i[3] \sim U(0, 2\pi); & i < d_g/2 \\ \psi_i[1] = 0, \quad \psi_i[2] \sim U(0, 50), \quad \psi_i[3] \sim U(0, 2\pi); & i \geq d_g/2 \end{cases}, \quad (10)$$

where $U(\cdot)$ denotes the uniform distribution. We use an AdamW optimiser [28] with a learning rate of 0.01, conducting 1,000 epochs of training and selecting the functions with the minimum training error as final. For GMT training, we employ AdamW with an initial learning rate of 0.0001 and a batch size of 12 across all datasets. Specifically, for CVPPP LSC A1, the training lasts 1,000 epochs with learning rate reductions by a factor of 0.1 at epochs 900 and 950. For KOMATSUNA RGB and MSU-PID, GMT is trained for 200 epochs, with learning rate multiplying by 0.1 at epoch 50 and 150. Models demonstrating optimal performance on the validation set are chosen as the final test models.

Evaluation Metrics. We evaluate our approach using three standard metrics widely adopted for leaf instance segmentation: Best Dice (BD), Symmetric Best Dice (SBD), and Difference in Count (IDiC). Further details on these metrics can be found in Scharr *et al.* [63].

4.3 Quantitative and Qualitative Results

The results on CVPPP LSC A1, MSU-PID Arabidopsis and KOMATSUNA RGB are presented on Tables 1 and 2, with qualitative results shown in Figure 4. For all three datasets, we observe that Mask2Former (COCO pre-trained) already surpass previous SotA approaches, so we mainly compare Mask2Former with the proposed GMT.

³For GMT, we load the COCO pre-trained weights from Mask2Former, omitting the incompatible keys.

Table 1: CVPPP LSC A1 test set results. The star symbol (*) indicates our implementation, while other results were taken from [0].

	SBD ↑	lDiCl ↓
Discriminative [10]	79.6	1.4
PEA [19]	83.8	2.4
SPOCO [59]	84.4	1.7
BISSG [26]	87.3	1.4
OGIS [40]	87.5	1.1
PCTrans [0]	88.7	0.7
Mask2Former* [9]	89.5	0.67
GMT (Ours)	90.1	0.48

Table 2: MSU-PID Arabidopsis [10] and KOMATSUNA RGB [55] test set results. The star symbol (*) indicates our implementation, while other results were taken from [0].

	BD ↑	SBD ↑	lDiCl ↓
<i>MSU-PID Arabidopsis</i> [10]			
Yin <i>et al.</i> [40]	65.2	\	\
Eff-Unet++ [0]	71.2	\	\
Mask2Former* [9]	85.7	83.1	0.47
GMT (Ours)	86.1	83.5	0.47
<i>KOMATSUNA RGB</i> [55]			
Ward <i>et al.</i> [53]	62.4	\	\
UPGen [37]	77.8	\	\
Eff-Unet++ [0]	83.4	\	\
Mask2Former* [9]	93.5	90.9	0.2
GMT (Ours)	94	91	0.22

CVPPP LSC A1. We observe consistent performance enhancements of GMT compared to Mask2Former, showing improvements of +0.6 in SBD and +0.19 in lDiCl. In addition, GMT outperforms Mask2Former in BD (91.8 vs 91).

MSU-PID Arabidopsis. Table 2 shows that GMT surpass Mask2Former by +0.4 on BD and SBD, respectively, while performing on par in lDiCl.

KOMATSUNA RGB. GMT shows clear improvement over Mask2Former in BD by +0.5, slightly outperforms in SBD by +0.1, while slightly underperforms in lDiCl by -0.02.

In summary, the proposed GMT outperforms the SotA models on all three datasets. GMT also surpass the standard Mask2Former in most scenarios (except for the lDiCl in KOMATSUNA RGB). To further demonstrate the superiority of GMT over Mask2Former, the next section showcases an ablation study.

4.4 Ablation Study

Ablative experiments are performed on CVPPP LSC A1, with performance reported on the hidden test set. Firstly, we assess different backbone models with results in Table 3. We find that the smallest model (ResNet-50) achieves the best SBD and lDiCl, while the largest model (SwinT-Base) reaches the best BD. As SBD is the lower bound of BD, these results

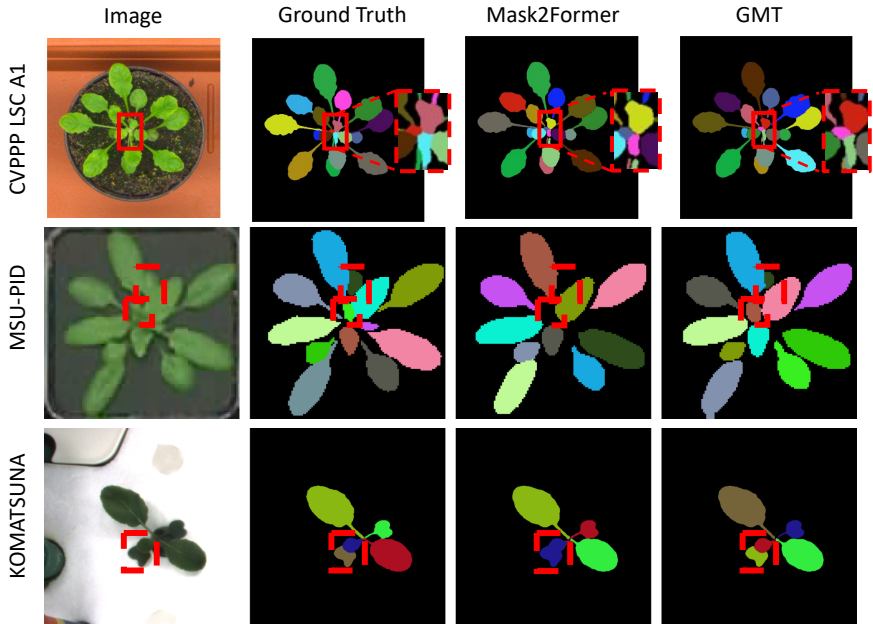


Figure 4: Qualitative results on the CVPPP A1 validation set, the MSU-PID test set, and the KOMATSUNA test set.

Table 3: Performance of our method with different backbones.

Backbone	BD \uparrow	SBD \uparrow	lDiCl \downarrow
SwinT-Base	92.2	89.9	0.7
ResNet-101	92.1	89.3	0.73
ResNet-50	91.8	90.1	0.48

Table 4: Performance of our method when key components are removed.

Component	BD \uparrow	SBD \uparrow	lDiCl \downarrow
w/o GPE	91.0	88.0	0.76
w/o GEFM	90.6	89.5	0.55
w/o GDPQ	91.5	89.3	0.73
GMT	91.8	90.1	0.48

indicate that using SwinT-Base may be able to produce higher-quality leaf masks for some instances, while ResNet-50 generalises more broadly.

Next, we assess the performance of GMT by removing each individual components (*c.f.* Section 3), to identify their impact on performance. The results in Table 4 indicate that each component is crucial in the overall performance of GMT.

5 Conclusion

In this paper, we present the Guided Mask Transformer (GMT): a Transformer-based leaf instance segmentation model tailored to plant images. GMT contains three novel components, namely Guided Positional Encoding (GPE), Guided Embedding Fusion Module (GEFM), and Guided Dynamic Positional Queries (GDPQ), to effectively integrate with a set of guide functions possessing spatial priori of leaf instances. We demonstrate the effectiveness of our

approach in three widely used plant phenotyping datasets, showing that GMT is able to outperform the SotA. We also show the efficacy of each key component via the ablation study. Our future work should focus on extending GMT to work on more challenging scenarios (e.g. in-field plant image analysis) in plant science and the broader biology community.

References

- [1] Hangbo Bao, Li Dong, Songhao Piao, and Furu Wei. Beit: Bert pre-training of image transformers. *arXiv preprint arXiv:2106.08254*, 2021.
- [2] Sandesh Bhagat, Manesh Kokare, Vineet Haswani, Praful Hambarde, and Ravi Kamble. Eff-unet++: A novel architecture for plant leaf segmentation and counting. *Ecological Informatics*, 68:101583, 2022.
- [3] Tom Brown, Benjamin Mann, Nick Ryder, Melanie Subbiah, Jared D Kaplan, Prafulla Dhariwal, Arvind Neelakantan, Pranav Shyam, Girish Sastry, Amanda Askell, et al. Language models are few-shot learners. *Advances in neural information processing systems*, 33:1877–1901, 2020.
- [4] Nicolas Carion, Francisco Massa, Gabriel Synnaeve, Nicolas Usunier, Alexander Kirillov, and Sergey Zagoruyko. End-to-end object detection with transformers. In *European conference on computer vision*, pages 213–229. Springer, 2020.
- [5] Feng Chen, Mario Valerio Giuffrida, and Sotirios A Tsafaris. Adapting vision foundation models for plant phenotyping. In *Proceedings of the IEEE/CVF International Conference on Computer Vision*, pages 604–613, 2023.
- [6] Kai Chen, Jiangmiao Pang, Jiaqi Wang, Yu Xiong, Xiaoxiao Li, Shuyang Sun, Wansen Feng, Ziwei Liu, Jianping Shi, Wanli Ouyang, et al. Hybrid task cascade for instance segmentation. In *Proceedings of the IEEE/CVF conference on computer vision and pattern recognition*, pages 4974–4983, 2019.
- [7] Qi Chen, Wei Huang, Xiaoyu Liu, Jiacheng Li, and Zhiwei Xiong. Pctrans: Position-guided transformer with query contrast for biological instance segmentation. In *Proceedings of the IEEE/CVF International Conference on Computer Vision*, pages 3903–3912, 2023.
- [8] Bowen Cheng, Alex Schwing, and Alexander Kirillov. Per-pixel classification is not all you need for semantic segmentation. *Advances in neural information processing systems*, 34:17864–17875, 2021.
- [9] Bowen Cheng, Ishan Misra, Alexander G Schwing, Alexander Kirillov, and Rohit Girdhar. Masked-attention mask transformer for universal image segmentation. In *Proceedings of the IEEE/CVF conference on computer vision and pattern recognition*, pages 1290–1299, 2022.
- [10] Jeffrey A Cruz, Xi Yin, Xiaoming Liu, Saif M Imran, Daniel D Morris, David M Kramer, and Jin Chen. Multi-modality imagery database for plant phenotyping. *Machine Vision and Applications*, 27:735–749, 2016.

- [11] Bert De Brabandere, Davy Neven, and Luc Van Gool. Semantic instance segmentation with a discriminative loss function. *arXiv preprint arXiv:1708.02551*, 2017.
- [12] Jacob Devlin, Ming-Wei Chang, Kenton Lee, and Kristina Toutanova. Bert: Pre-training of deep bidirectional transformers for language understanding. *arXiv preprint arXiv:1810.04805*, 2018.
- [13] Alexey Dosovitskiy, Lucas Beyer, Alexander Kolesnikov, Dirk Weissenborn, Xiaohua Zhai, Thomas Unterthiner, Mostafa Dehghani, Matthias Minderer, Georg Heigold, Sylvain Gelly, et al. An image is worth 16x16 words: Transformers for image recognition at scale. *arXiv preprint arXiv:2010.11929*, 2020.
- [14] Ruiming Du, Zhihong Ma, Pengyao Xie, Yong He, and Haiyan Cen. Pst: Plant segmentation transformer for 3d point clouds of rapeseed plants at the podding stage. *ISPRS Journal of Photogrammetry and Remote Sensing*, 195:380–392, 2023.
- [15] Abdul Mueed Hafiz and Ghulam Mohiuddin Bhat. A survey on instance segmentation: state of the art. *International journal of multimedia information retrieval*, 9(3):171–189, 2020.
- [16] Haoyu He, Jianfei Cai, Zizheng Pan, Jing Liu, Jing Zhang, Dacheng Tao, and Bohan Zhuang. Dynamic focus-aware positional queries for semantic segmentation. In *Proceedings of the IEEE/CVF Conference on Computer Vision and Pattern Recognition*, pages 11299–11308, 2023.
- [17] Junjie He, Pengyu Li, Yifeng Geng, and Xuansong Xie. Fastinst: A simple query-based model for real-time instance segmentation. In *Proceedings of the IEEE/CVF Conference on Computer Vision and Pattern Recognition*, pages 23663–23672, 2023.
- [18] Kaiming He, Xiangyu Zhang, Shaoqing Ren, and Jian Sun. Deep residual learning for image recognition. In *Proceedings of the IEEE conference on computer vision and pattern recognition*, pages 770–778, 2016.
- [19] Wei Huang, Shiyu Deng, Chang Chen, Xueyang Fu, and Zhiwei Xiong. Learning to model pixel-embedded affinity for homogeneous instance segmentation. In *Proceedings of the AAAI Conference on Artificial Intelligence*, volume 36, pages 1007–1015, 2022.
- [20] Jitesh Jain, Jiachen Li, Mang Tik Chiu, Ali Hassani, Nikita Orlov, and Humphrey Shi. Oneformer: One transformer to rule universal image segmentation. In *Proceedings of the IEEE/CVF Conference on Computer Vision and Pattern Recognition*, pages 2989–2998, 2023.
- [21] Weikuan Jia, Zhonghua Zhang, Wenjing Shao, Sujuan Hou, Ze Ji, Guoliang Liu, and Xiang Yin. Foveamask: A fast and accurate deep learning model for green fruit instance segmentation. *Computers and Electronics in Agriculture*, 191:106488, 2021.
- [22] Kan Jiang, Usman Afzaal, and Joonwhoan Lee. Transformer-based weed segmentation for grass management. *Sensors*, 23(1):65, 2022.
- [23] Victor Kulikov and Victor Lempitsky. Instance segmentation of biological images using harmonic embeddings. In *Proceedings of the IEEE/CVF Conference on Computer Vision and Pattern Recognition*, pages 3843–3851, 2020.

- [24] Zhenbo Li, Ruohao Guo, Meng Li, Yaru Chen, and Guangyao Li. A review of computer vision technologies for plant phenotyping. *Computers and Electronics in Agriculture*, 176:105672, 2020. ISSN 0168-1699. doi: <https://doi.org/10.1016/j.compag.2020.105672>. URL <https://www.sciencedirect.com/science/article/pii/S0168169920307511>.
- [25] Tsung-Yi Lin, Michael Maire, Serge Belongie, James Hays, Pietro Perona, Deva Ramanan, Piotr Dollár, and C Lawrence Zitnick. Microsoft coco: Common objects in context. In *Computer Vision—ECCV 2014: 13th European Conference, Zurich, Switzerland, September 6–12, 2014, Proceedings, Part V 13*, pages 740–755. Springer, 2014.
- [26] Xiaoyu Liu, Wei Huang, Yueyi Zhang, and Zhiwei Xiong. Biological instance segmentation with a superpixel-guided graph. In *IJCAI*, pages 1209–1215, 2022.
- [27] Ze Liu, Yutong Lin, Yue Cao, Han Hu, Yixuan Wei, Zheng Zhang, Stephen Lin, and Baining Guo. Swin transformer: Hierarchical vision transformer using shifted windows. In *Proceedings of the IEEE/CVF international conference on computer vision*, pages 10012–10022, 2021.
- [28] Ilya Loshchilov and Frank Hutter. Decoupled weight decay regularization. *arXiv preprint arXiv:1711.05101*, 2017.
- [29] Fausto Milletari, Nassir Navab, and Seyed-Ahmad Ahmadi. V-net: Fully convolutional neural networks for volumetric medical image segmentation. In *2016 fourth international conference on 3D vision (3DV)*, pages 565–571. Ieee, 2016.
- [30] Shervin Minaee, Yuri Boykov, Fatih Porikli, Antonio Plaza, Nasser Kehtarnavaz, and Demetri Terzopoulos. Image segmentation using deep learning: A survey. *IEEE transactions on pattern analysis and machine intelligence*, 44(7):3523–3542, 2021.
- [31] Massimo Minervini, Andreas Fischbach, Hanno Schar, and Sotirios A Tsaftaris. Finely-grained annotated datasets for image-based plant phenotyping. *Pattern recognition letters*, 81:80–89, 2016.
- [32] William Peebles and Saining Xie. Scalable diffusion models with transformers. In *Proceedings of the IEEE/CVF International Conference on Computer Vision*, pages 4195–4205, 2023.
- [33] Hanno Schar, Massimo Minervini, Andrew P French, Christian Klukas, David M Kramer, Xiaoming Liu, Imanol Luengo, Jean-Michel Pape, Gerrit Polder, Danijela Vukadinovic, et al. Leaf segmentation in plant phenotyping: a collation study. *Machine vision and applications*, 27:585–606, 2016.
- [34] Vijai Singh and Ak K Misra. Detection of plant leaf diseases using image segmentation and soft computing techniques. *Information processing in Agriculture*, 4(1):41–49, 2017.
- [35] Hideaki Uchiyama, Shunsuke Sakurai, Masashi Mishima, Daisaku Arita, Takashi Okayasu, Atsushi Shimada, and Rin-ichiro Taniguchi. An easy-to-setup 3d phenotyping platform for komatsuna dataset. In *Proceedings of the IEEE international conference on computer vision workshops*, pages 2038–2045, 2017.

- [36] Ashish Vaswani, Noam Shazeer, Niki Parmar, Jakob Uszkoreit, Llion Jones, Aidan N Gomez, Łukasz Kaiser, and Illia Polosukhin. Attention is all you need. *Advances in neural information processing systems*, 30, 2017.
- [37] Daniel Ward and Peyman Moghadam. Scalable learning for bridging the species gap in image-based plant phenotyping. *Computer Vision and Image Understanding*, 197: 103009, 2020.
- [38] Daniel Ward, Peyman Moghadam, and Nicolas Hudson. Deep leaf segmentation using synthetic data. *arXiv preprint arXiv:1807.10931*, 2018.
- [39] Adrian Wolny, Qin Yu, Constantin Pape, and Anna Kreshuk. Sparse object-level supervision for instance segmentation with pixel embeddings. In *Proceedings of the IEEE/CVF Conference on Computer Vision and Pattern Recognition*, pages 4402–4411, 2022.
- [40] Jingru Yi, Pengxiang Wu, Hui Tang, Bo Liu, Qiaoying Huang, Hui Qu, Lianyi Han, Wei Fan, Daniel J Hoepfner, and Dimitris N Metaxas. Object-guided instance segmentation with auxiliary feature refinement for biological images. *IEEE Transactions on Medical Imaging*, 40(9):2403–2414, 2021.
- [41] Xi Yin, Xiaoming Liu, Jin Chen, and David M Kramer. Joint multi-leaf segmentation, alignment, and tracking for fluorescence plant videos. *IEEE transactions on pattern analysis and machine intelligence*, 40(6):1411–1423, 2017.
- [42] Jiajing Zhang, An Min, Brian J Steffenson, Wen-Hao Su, Cory D Hirsch, James Anderson, Jian Wei, Qin Ma, and Ce Yang. Wheat-net: An automatic dense wheat spike segmentation method based on an optimized hybrid task cascade model. *Frontiers in Plant Science*, 13:834938, 2022.
- [43] Xizhou Zhu, Weijie Su, Lewei Lu, Bin Li, Xiaogang Wang, and Jifeng Dai. Deformable detr: Deformable transformers for end-to-end object detection. *arXiv preprint arXiv:2010.04159*, 2020.

A Supplementary Materials

A.1 Loss Function of GMT

The loss function of the proposed Guided Mask Transformer (GMT) is defined as:

$$L = \lambda_{\text{ce}}L_{\text{ce}} + \lambda_{\text{dice}}L_{\text{dice}} + \lambda_{\text{cls}}L_{\text{cls}} + \lambda_{\text{guide}}L_{\text{guide}}, \quad (11)$$

where λ_x denotes the weight of the corresponding loss L_x . The first three terms are consistent with the standard Mask2Former [9], where L_{ce} and L_{dice} represent the binary cross-entropy loss and the dice loss [29] for mask prediction, respectively. L_{cls} is the cross-entropy loss for classification. The last term L_{guide} is an L_1 loss applied to the guided features, as referenced at the Guided Embedding Fusion Module (GEFM) in Section 3.2 and Figure 2.

In our experiments, we set $\lambda_{\text{ce}} = 2$, $\lambda_{\text{dice}} = 5$, $\lambda_{\text{cls}} = 2$, and $\lambda_{\text{guide}} = 5$, respectively. The number of classes of L_{cls} is set to 1, to distinguish between leaves and background.

A.2 Mathematical Definition of Evaluation Metrics

In this section, we detail the mathematical definitions of the evaluation metrics utilized in our experiments, as referenced in Section 4.2.

We use three evaluation metrics: BEST DICE (BD), SYMMETRIC BEST DICE (SBD), and ABSOLUTE DIFFERENCE IN COUNT (lDiC), as defined in [53]. The generalised form of BD is defined as:

$$\text{BD}(Y^a, Y^b) = \frac{1}{M} \sum_{i=1}^M \max_{1 \leq j \leq N} \text{DICE}(Y_i^a, Y_j^b), \quad (12)$$

where Y^a and Y^b are two sets of instance masks, with M and N denoting the number of masks in Y^a and Y^b , respectively. The DICE score is defined as:

$$\text{DICE}(Y_i^a, Y_j^b) = \frac{2|Y_i^a \cap Y_j^b|}{|Y_i^a| + |Y_j^b|}, \quad (13)$$

where $|\cdot|$ indicates the number of pixels.

The BD between predicted instance masks \hat{Y} and ground-truth instance masks Y is calculated as $\text{BD}(\hat{Y}, Y)$, and the SBD is defined as:

$$\text{SBD}(\hat{Y}, Y) = \min \{ \text{BD}(\hat{Y}, Y), \text{BD}(Y, \hat{Y}) \}. \quad (14)$$

The final metric, lDiC, quantifying the difference between the predicted and ground-truth number of instances (*i.e.* leaves), is defined as:

$$|\text{DiC}| = |M - N|, \quad (15)$$

where the operator $|\cdot|$ here denotes the absolute operation.

A.3 Additional Qualitative Results

In this section, we provide additional visual results to supplement Figure 4 and Section 4.3. Figure 5 presents qualitative results on the MSU-PID Arabidopsis test set: Compared to the proposed GMT, Mask2Former [9] under-segments (Row 1) and misses (Rows 2 - 7) some leaves. Figure 6 shows qualitative results on the KOMATSUNA RGB test set: Compared to the proposed GMT, Mask2Former erroneously identifies green objects in the background as leaves (Rows 1 - 3) and under-segments some leaves (Rows 4 and 5).

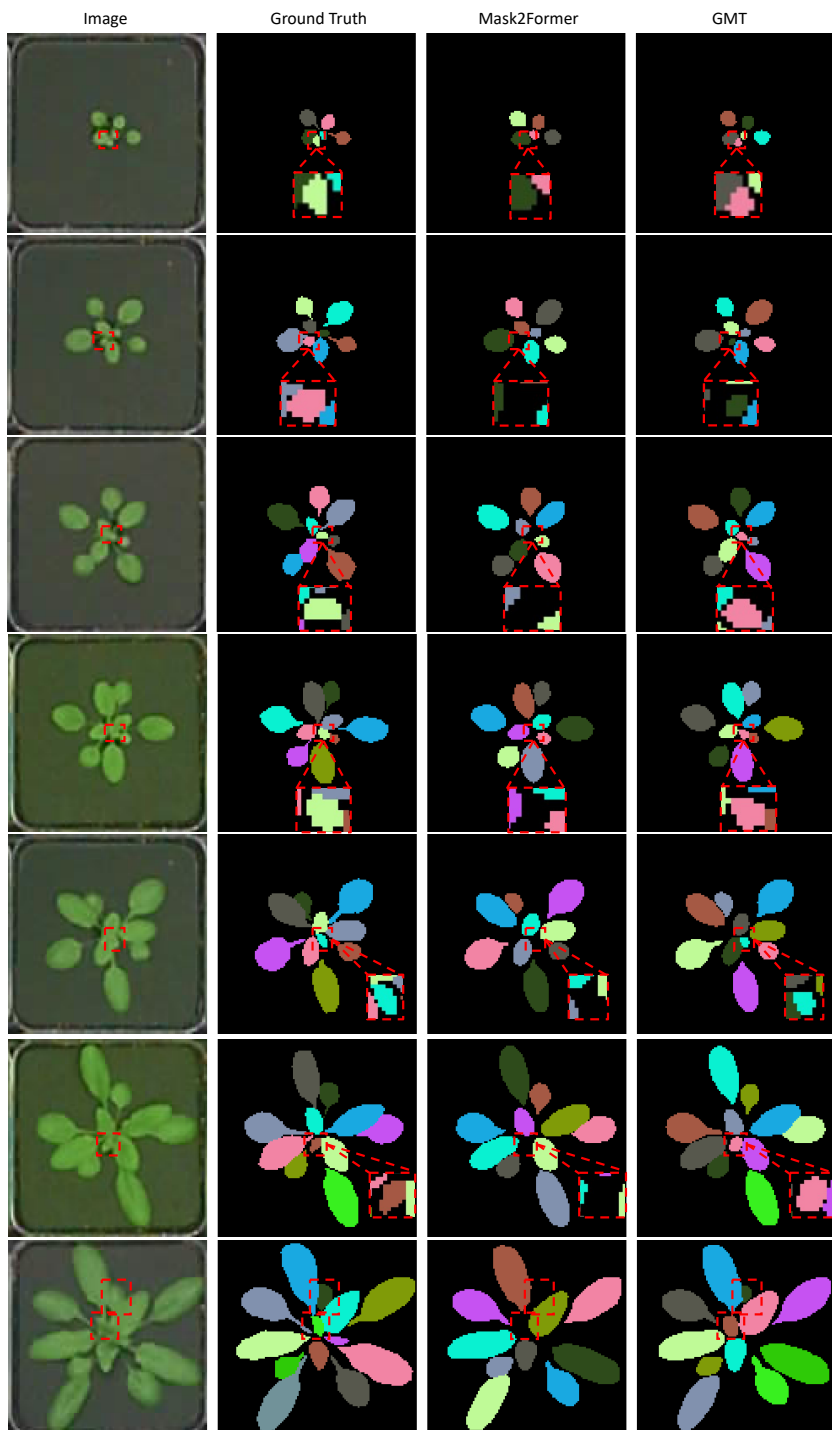


Figure 5: Qualitative results on MSU-PID Arabidopsis test set. The key difference between the predictions of Mask2Former [9] and our method (GMT) is highlighted in the red boxes.

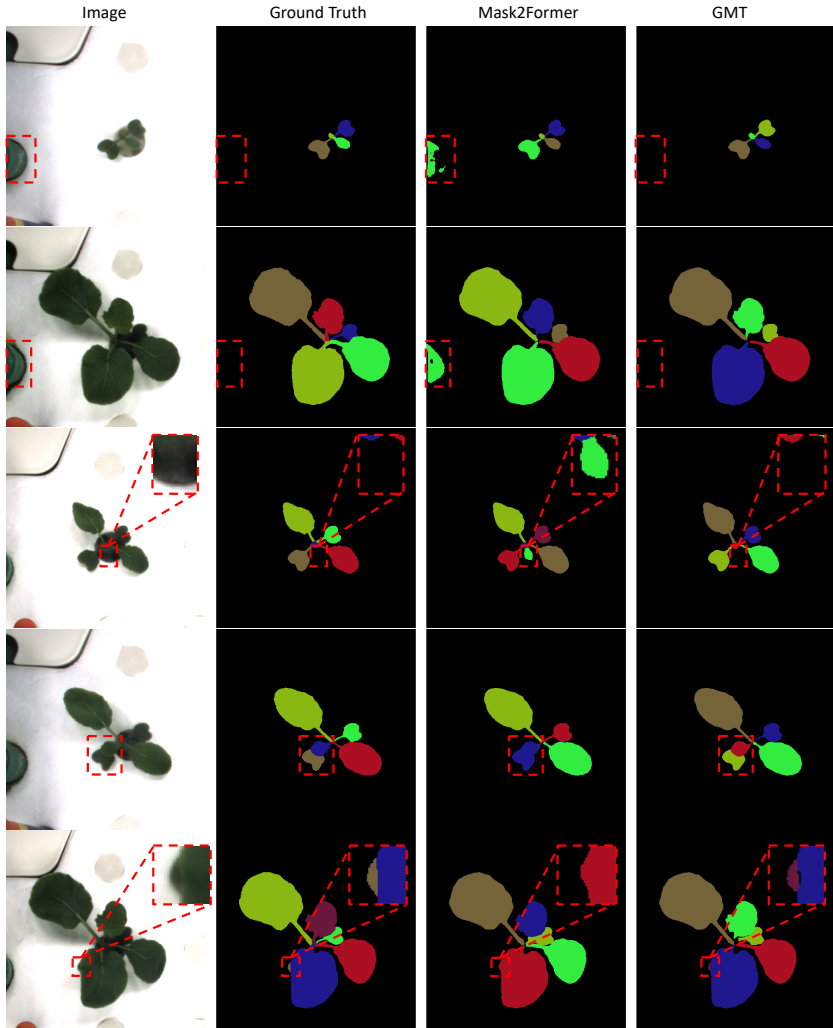


Figure 6: Qualitative results on KOMATSUNA RGB test set. The key difference between the predictions of Mask2Former [9] and our method (GMT) is highlighted in the red boxes.